The Growth and Dynamics of Brinicles

Abstract

Observations in the Arctic and Antarctic oceans show that where cold, dense brine is rejected from new sea ice, hollow ice formations, known as brinicles form around these streamers of brine. In an experimental study, we grew these brinicles in a tank maintained at its freezing temperature inside a freezer. We pumped brine at a fixed temperature and flow rate into this tank and recorded these brinicles growing. We grew and recorded these brinicles in tanks of differing salinities, ranging from completely fresh water to the salinity in McMurdo Sound, Antarctica (Martin, 1974). By analyzing these images in MatLab, we were able to detect the edges of these brinicles, and compare the lengths and widths to a model by Martin (1974). We were also able to compare these brinicles with aa new model, based on the thickness of the walls of the brinicle. The shape of these brinicles was also analyzed, and we saw that as the salinity of the water in which they grew increased, the structure of the brincles changed. In more saline water, the ice crystals in the brinicles were oriented radially, the brinicles were much more fragile and prone to falling apart, and the outer edges appear smoother.

1 Introduction

Sea ice covers up to 12% of the surface area of the ocean during the winter months, which is 7% of the total surface area of the planet (Weeks, 1967). Since the ice has a bright, reflective surface, especially in comparison to the dark ocean around it, so large portions of the polar regions reflect back most of the incoming solar energy and causing the rest of the planet to cool. As sea ice melts, there is less of a reflective surface and more heat is absorbed, which leads to the ice melting faster. Because of this, a slight shift in temperature can lead to a large amount of ice melting and overall warming. While some of this sea ice is permanent and persists all year, much of it freezes every winter. As seawater freezes, the ice formed has a much lower salinity than the water it freezes from. The salt is rejected from freezing ice in the form of cold, dense brine that sinks towards the ocean floor. As large volumes of this brine sink, it contributes to the ocean's global circulation. Cold, denser water flows along the ocean floor away from the poles, while warmer water flows from the equator towards the poles (National Snow and Ice Data Center, 2017).

To understand the dynamics of freezing, we must turn to concepts from the materials science of solidification. The binary phase diagram (fig. 1.1) tells us what phases exist in a mixture of a given concentration and temperature. The line separating the liquid and crystalline solid + liquid phases is called the liquidus and is highlighted in fig. 1.1. The point at which the two liquidus lines join is the eutectic point. For a sample at a particular concentration and temperature there exists an equilibrium with a fraction of solid phase and a fraction of liquid phase. As sea ice forms, it exists continuously in near-equilibrium states. At equilibrium, pure ice and brine exist together at a ratio determined by the binary phase diagram (Worster, 2000). Ideally, sea ice would freeze and result in a perfect sheet of pure ice over salt-water where all the salt is rejected from the volume occupied by ice into the brine below. In actuality, sea ice initially starts out salty, and over time the salinity

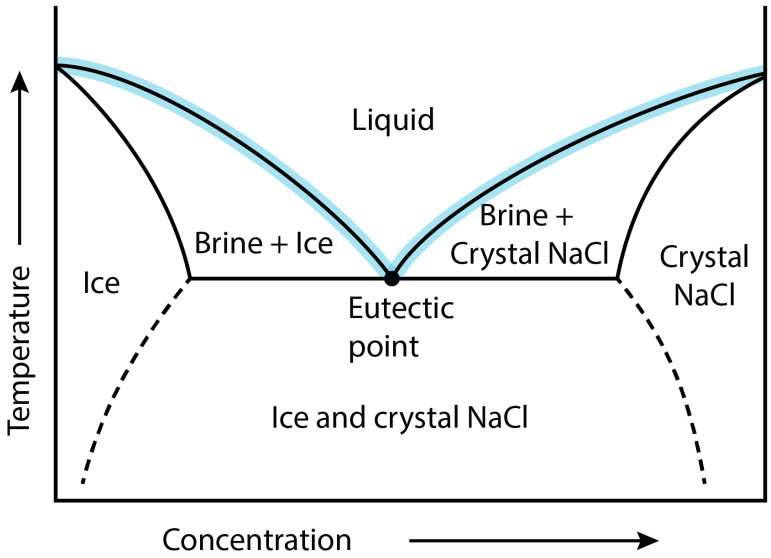

Figure 1.1: The general binary phase diagram that shows the phase for a given concentration and temperature)

decreases (Weeks, 1967). The salinity decreases as brine drains out of brine pockets and mushy regions, into the water below. This brine is much colder and more saline than the ocean water below, as the seawater freezes from the top down due to air temperatures of $-10°$C and lower (Perovich et al., 1995). This sinking brine flows into the seawater below in volumes of anywhere from 1.3 to 18 mL/sec depending on the conditions, as observed by Perovich et al. (1995) and Dayton and Martin (1971). Heat can only flow into the brine from the surrounding fresh water, which then freezes into the wall of the brinicle. As a large volume of brine flows in, the brinicle continues to freeze and to grow in both length and width. Both the inner and the outer radius of the structure grow with time. As the brinicle freezes and the outer wall grows, heat is transferred across the ice wall to a layer of warmer brine along the inner wall of the brinicle. This warmer brine then dissolves the inner wall, bringing it back to the liquidus. The outer wall grows as heat flows to the cold brine at the center, freezing the fluid at the outer wall. In this way, both the inner and the

outer wall of the brinicle grow with time.

An interesting free-boundary problem arises in characterizing these brinicles. Multiple phenomena, including heat transfer, diffusion of solutes across concentration gradients, and phase changes, intersect in the occurrence of brinicles. The impact of these brinicles, however goes beyond just interesting physics. The process by which salty brine escapes sea ice is a topic of significant research as it impacts the growth of sea ice and the mixing of the Arctic Ocean. The presence of these brinicles could help to throw light on this process in some ways. Formation of these brinicles has been connected with the deformation of thin, new sea ice. This highly saline ice has few, small brinicles growing below it, but when it rafts and attaches to another ice sheet, the brine drained rapidly from the growing ice and brinicles grew to a length of 2m (Perovich et al., 1995). Finally, this problem is not already very well investigated, with only handful of publications touching upon brinicles in the last few decades.

2 Experiment

To understand the growth of brinicles in a laboratory setting, we carried out an experiment based on the study by S. Martin in 1972. We conducted this experiment inside a freezer, which was maintained between -17° C and -20° C. The brinicle was grown in a tank inside this freezer; this tank remained at its freezing temperature. A box filled with ice was fixed to the top of the tank, and brine was pumped through a hole in this ice order to to grow the brinicle as shown in fig. 2.1. The brine was stored in an open container in the freezer and pumped with a peristaltic pump into the tank. In order to increase the salinity of the tank, first a brinicle was grown in fresh water. Then the block of ice, pump, and brinicle were removed and salt added to the tank. The salt was dissolved by running a submersible pump in the tank, and the seawater was observed to be at its freezing temperature by

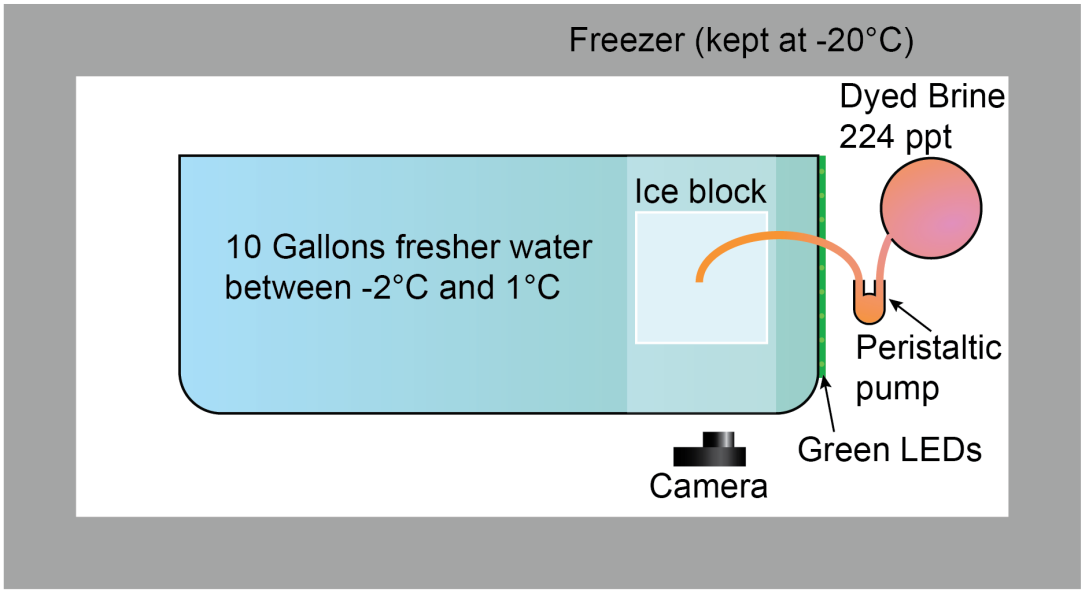

Figure 2.1: The experimental setup, as viewed from above.

the presence of small ice crystals as well as the fact that the measured temperature of the tank remained constant. Once again, the block of ice was fixed to the top of the tank, and more brine pumped in to grow a second brinicle in the saltier water. This process was repeated to iterate through different salinities, each time letting the tank reach its new freezing temperature after the salt was added.

The experiment was conducted in a tank with a black background, lit from the side with LED lights, and filmed at 90° from the lights, in the front. Up to four images were taken per second, and the pump stopped shortly after the brinicle's tip went out of the frame of the camera. In order to more clearly see the outline and features of the brinicle, the images were processed by taking a running median for every pixel in MatLab over 8 second intervals, and subtracting the first frame, as the background.

A threshold was then applied to the images shown in fig. 2.2 and the edges of the

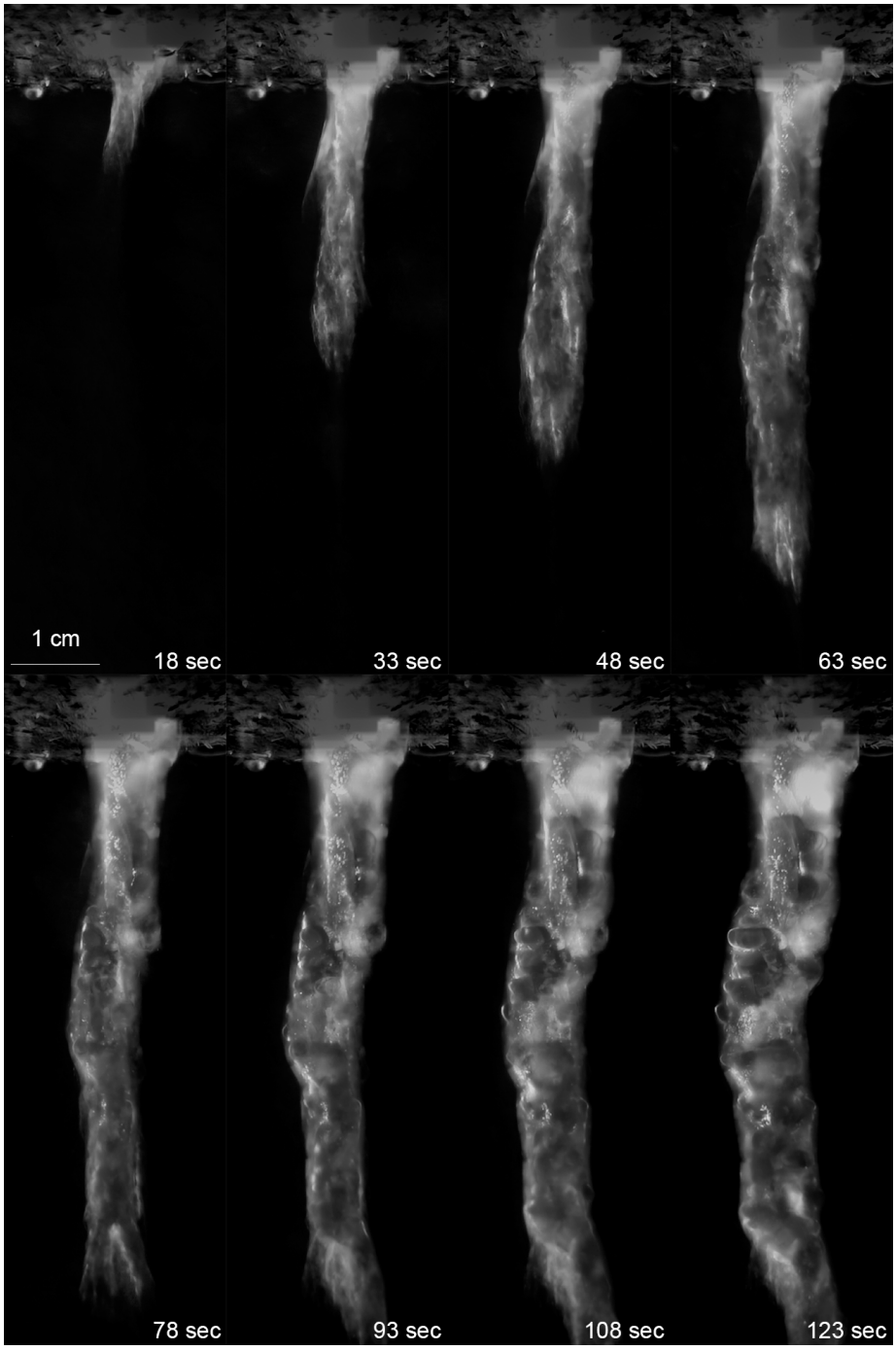

Figure 2.2: A sequence of photographs showing the growth of a brinicle. Salinity=22.4%, T=-19.4 degrees C

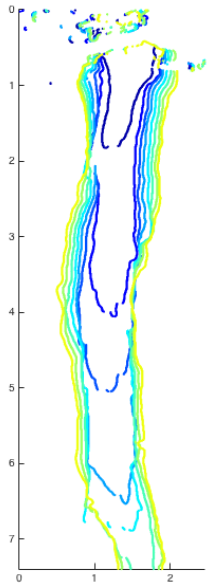

Figure 2.3: The edge of the brinicle as found by the edge-detection in MatLab, plotted at the same time steps as in (2.2)

brinicle detected in MatLab based on the derivative of changing color. From these edges we could then see where the tip was at every point in time, as well as the width at any given height and time in the lab frame. In order to visualize the growth of the brinicle in both length and width we can plot this width as a function of the height and time as seen in fig. 2.5a. We can easily see the tip at the boundary between the brinicle having zero and a positive width.

The schematic in fig. 2.4 shows this boundary, as well as the increasing width and location in the tank. We can see clearly here the structure of these plots that display the width (in color) as a function of both the time and the height in the lab frame, as filmed by the camera.

We can then plot the position of the tip as a function of time, and in order to check that

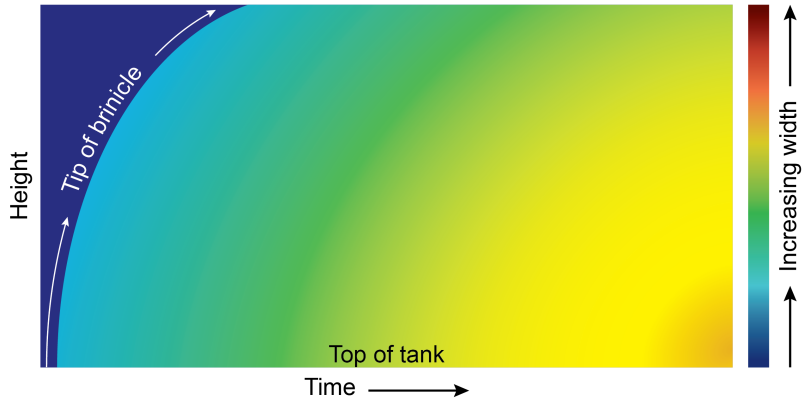

Figure 2.4: A schematic showing the way the brinicle grows in this type of space-time plot

the power law found by Martin holds, plot this on a log-log plot. We see in fig. 2.6 that the tip grows with $\sqrt{t}$, as predicted by Martin (1974). At earlier times the rate of growth of the brinicle fluctuates; we see regions of slow growth and even a region of particularly rapid growth. As time passes, however, the slope eventually reaches the predicted value.

We can also plot the width at a given height over time. However, at any given height, $t = 0$ occurs when the tip of the brinicle travels through that height. We can shift t_0 in two ways: either by the actual time that the tip travels through a given height, as shown in fig. 2.8 or we can first fit a polynomial to the position of the tip as it depends on time, and shift our t_0 based on that function, as shown in fig. 2.7. We can see that figures 2.8 and 2.7 shows two regimes of growth, although we see this in different ways in both plots. We can clearly see two different slopes in fig. 2.8 and in fig. 2.7, we see a region with a larger spread before the widths collapse onto each other. From this spread at earlier times and the collapse at later times, we can conclude that while the position of the tip may not always move as ideally as predicted, the width as a function of time is more robust.

From looking at both the images in fig. 2.2 and the edges in fig. 2.3, we can see that the

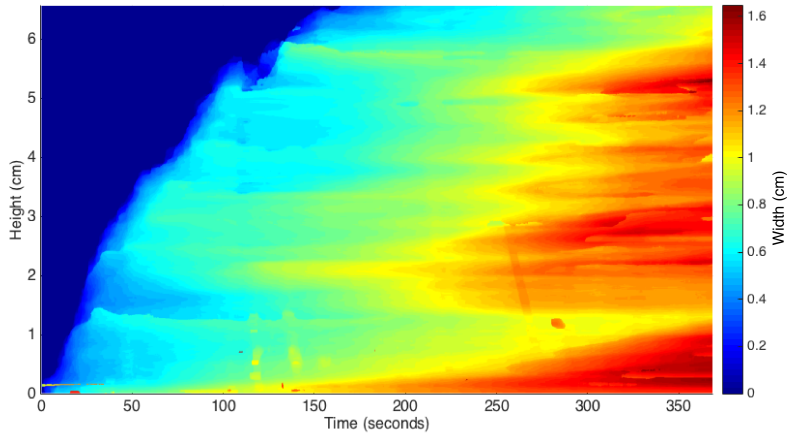

(a) The width of the brinicle at any given distance from the top (height) and time is shown by color on this plot. We can see the brinicle growing in both length and width, as well as see the growth of 'bumps' along the side of the brinicle.

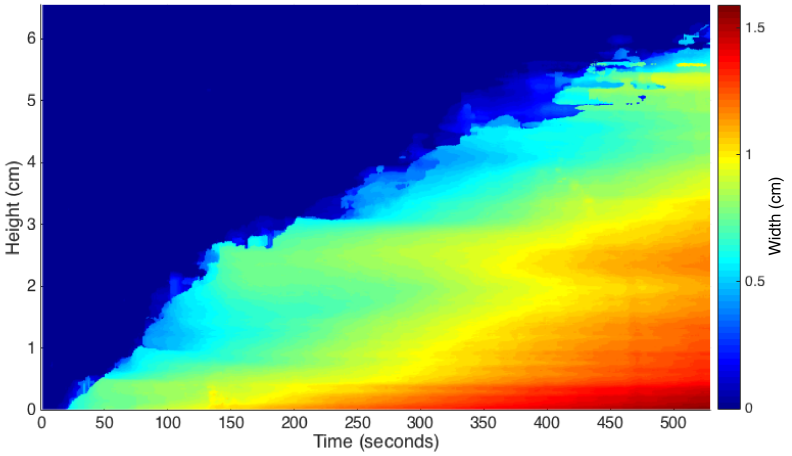

(b) The width of the brinicle at any given distance from the top (height) and time is shown by color on this plot. We can see the brinicle growing in both length and width. In this case, the brinicle was grown in salt water, and we can see fewer 'bumps' and less variation as the height changes.

Figure 2.5

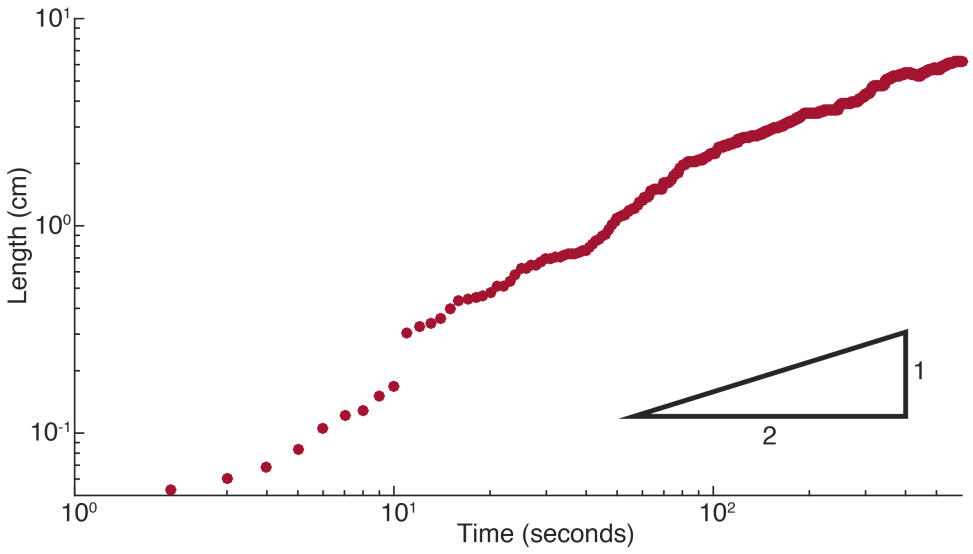

Figure 2.6: The length of a given brinicle plotted as a function of time on a log-log plot in order to see the dependence on $\sqrt{t}$

length and width are not the only ways of characterizing these brinicles. The shape evolves over time as well. Simply observationally, we can see that 'bumps' develop over time on the outer edge of these brinicles. In the photographs, we can see these on the front as well as the sides. These bumps form from an instability that can be reduced by increasing the salinity of the tank in which the brinicles are grown in. We can see in fig. 2.9 that this is the case: the structure of the brinicle grown in 3% salt water is drastically different from that grown in fresh water. Not only do we see far fewer bumps and smoother edges, but we can also see the increasing presence of radially-oriented ice crystals, as observed in nature by Perovich et al. (1995).

We also see that the brinicles grown in increasingly saline water grow slower. This makes sense, given that we now have dissolution of ice at both the outer and inner boundaries. When we plot the length of each brinicle in fig. 2.10a we can see that, for the most part, it takes more time for a brinicle grown in salt water to reach a certain length than a

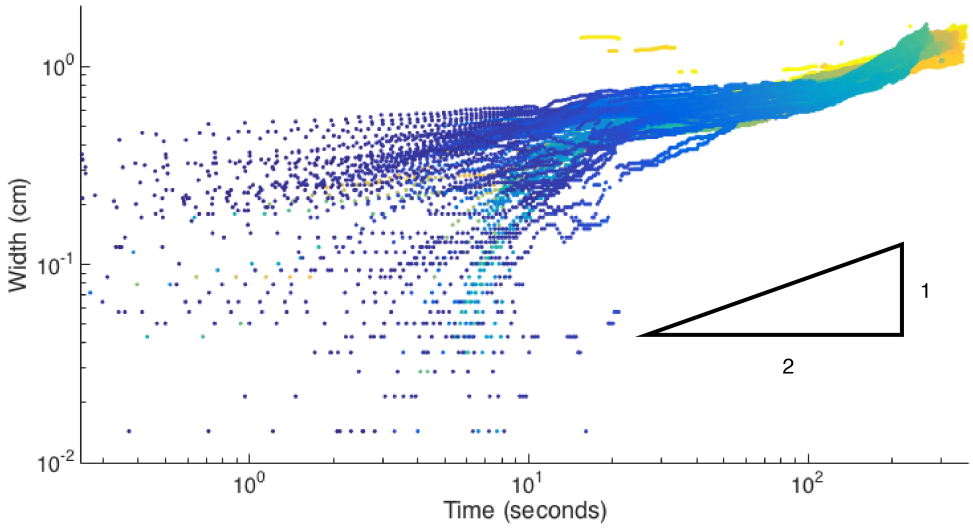

Figure 2.7: The width of the brinicle at given heights plotted as a function of time. At each height, $t = 0$ is shifted such that it is the time when the tip of the brinicle passes through that height, according to the power law fit to the tip. Each data point is colored based on its distance from the tip of the brinicle, divided by the total length of the brinicle.

brinicle grown in fresh water. Fig. 2.10a shows us that the shape of each growth curve is similar, although we can see that for each salinity the curve is shifted in a slightly different place. We see this in fig. 2.10b as well: all four lines appear to have the same slope, but different intercepts. If we were to quantify this, we would say that the term A_0 in front of $l(t) = A_0 t^{0.5}$ depends on the salinity of the tank. The addition of salt to the tank changes the condition that we wrote at the outer boundary; now, instead of the edge only freezing outward, there is also dissolving occurring.

When we plot the same data on a log-log plot and shift $t = 0$ for each brinicle to where that brinicle is 0.5 cm in length, as in fig. 2.10b, we can see that the the average of all four have the same slope. We quantify this roughness as deviation from the ideal. First, we fit a line using MatLab's polyfit to the edge of the brinicle as shown in fig. 2.11, and then calculate the root-mean-squared of the horizontal distance between that line and the edge

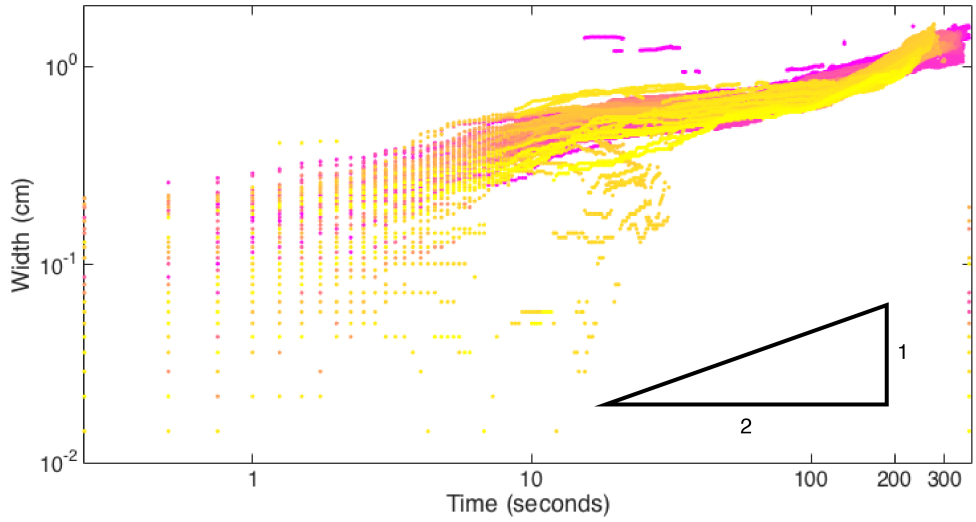

Figure 2.8: The width of the brinicle at given heights plotted as a function of time. At each height, $t = 0$ is shifted such that it is the first non-zero width at a given height, or where the tip actually passes through that point. Each data point is colored based on its height in the lab-space.

of the brinicle. We can do this for both the right and left edges of the brinicle, and average over a time range of 10 seconds. This gives us a number that defines the 'bumpiness' of each brinicle grown, which we can plot to see the relation with salinity.

As we see in fig. 2.10b, the addition of salt to the tank and therefore the dissolution on the outer boundary does not affect the rate of growth of the brinicle once growth has started. It does take slightly longer from when pumping begins for the brinicles in more saline water to begin growing; as ice crystals formed in the saline water dissolve, more loose ice crystals may form and not attach to the brinicle. This is also backed up by the observation of more loose floating ice crystals in tanks with higher salt concentration. The same dissolution applies to a thin sheet of ice, such as the wall of a new brinicle – it is dissolving from both sides, and therefore has to grow faster than it is dissolving in order to persist. So while the rate of growth of the tip is relatively unchanged despite the

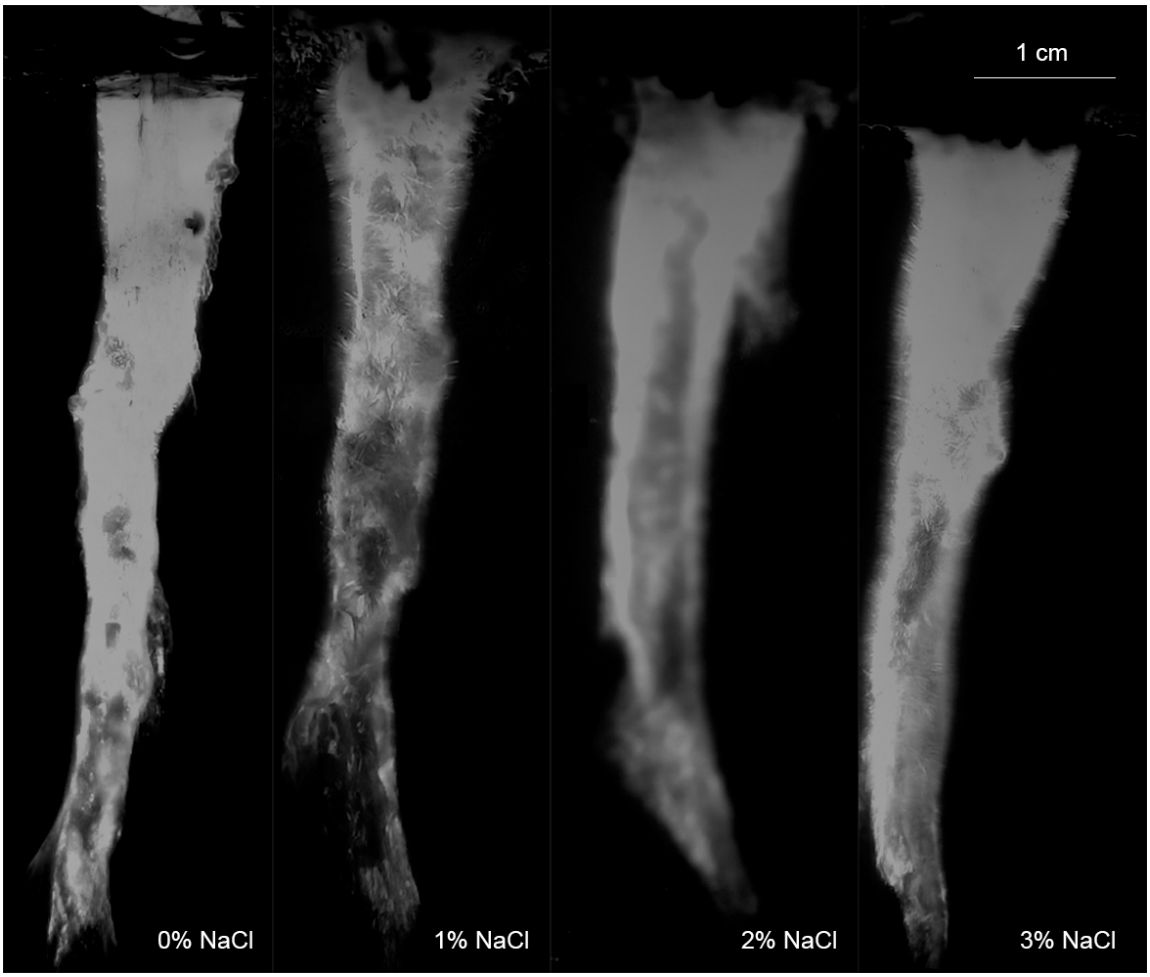

Figure 2.9: brinicles grown in tanks of different salinities and therefore different ambient temperatures as well. Salinity=22.4%

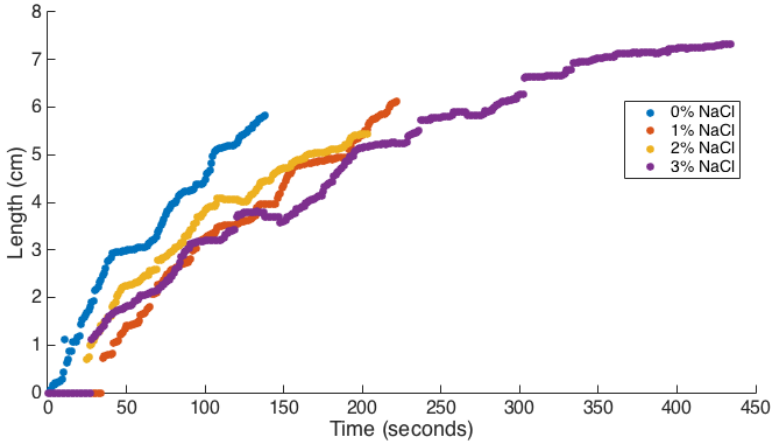

(a) The lengths with respect to time of four different brinicles, grown in tanks of varying salinity.

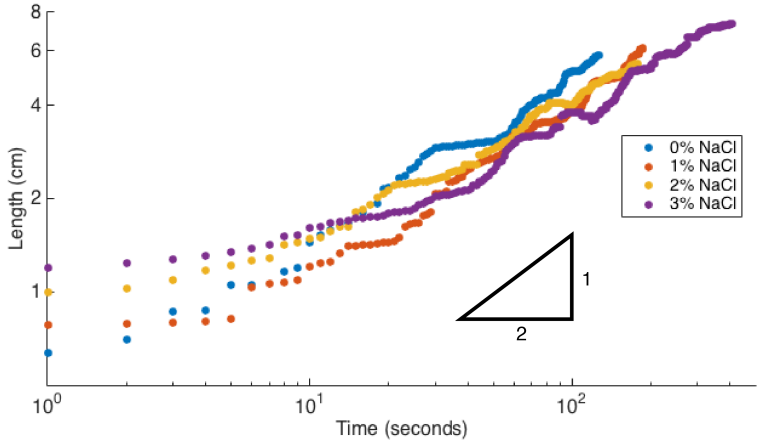

(b) The lengths of the same brinicles grown in different salinities, this time with each $t = 0$ when the brinicle is at a length of 0.5 cm

Figure 2.10

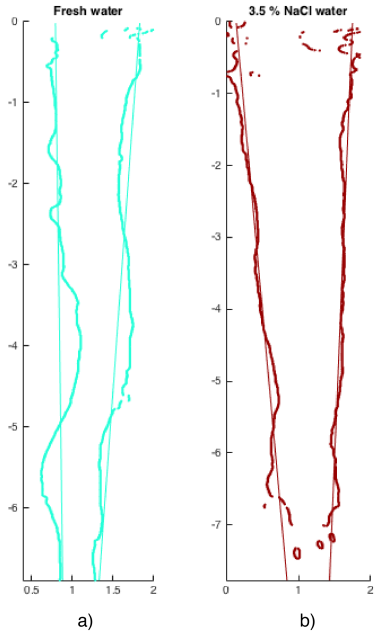

Figure 2.11: The shape of the brinicle grown in fresh water vs. seawater. a) In fresh water, the growth was uneven as can be seen from the deviation from a straight boundary. b) In salty water, the edges of the brinicle are more uniform

addition of salt, the increased salinity of the tank slows the growth of bumps on the side of the brinicle and changes the structure of crystals in the brinicle. We can see this both in the photographs of brinicles as well as quantitatively in fig. 2.12. This fig. confirms what we see just by looking at these photographs. While the data point at a salinity of 2% does not fit with the trend, the experimental conditions here were less than ideal – the camera did not focus and moved, and the brinicle changed its direction of growth, leaving a second, small brinicle, pointing in a different direction. Given more time, these experiments should be tried again under better conditions, and the brinicles grown longer so that the differences are more clearly visible.

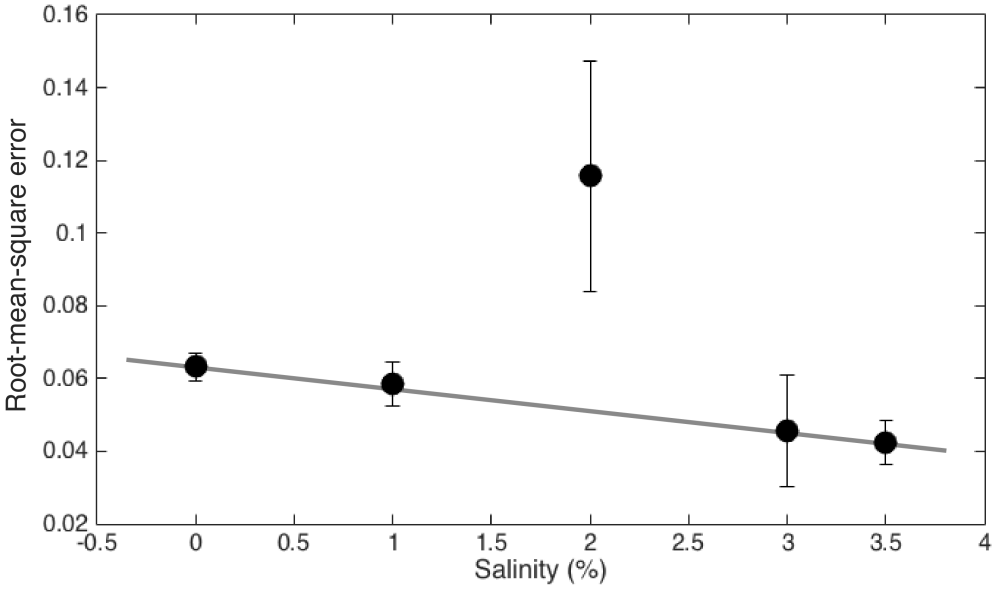

Figure 2.12: The root-mean-square error of the difference between the line fit and the actual edge of the brinicle, plotted as a function of salinity.

3 Model

A way of formulating solidification problems with a moving boundary is as a Stefan problem **?**. In this case, the boundary between ice and water moves as more ice freezes. This boundary moves as more ice crystals form in place and attach to the growing wall of ice. The simplest problem is where the whole system is held at T_m, the freezing temperature of the fluid. The frame can shift such that the boundary is held still and fluid flows towards it at rate V_n, the rate at which the boundary moves. We can create a control volume on the boundary, and write the balance of heat entering and exiting as follows

$$\rho H_l V_n - \underline{n} \cdot \underline{q}_l - \rho H_s V_n + \underline{n} \cdot \underline{q}_s = 0, \tag{1}$$

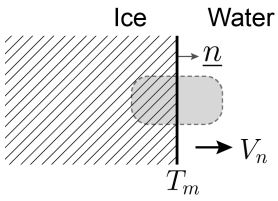

Figure 3.1: The advancing ice moves at speed V_n. The control volume is shown in gray.

Where ρ is the density, H is the enthalpy, $\underline{n}$ is a vector normal to the interface, and q is the heat flux.The first two terms correspond to heat flux into liquid, (l); the last two correspond to heat flux into the solid(s). Equation 1 can be rearranged to read:

$$\rho(H_l - H_s)V_n = \underline{n} \cdot \underline{q}_l - \underline{n} \cdot \underline{q}_s, \tag{2}$$

and simplified on noting that the latent heat of fusion $(\mathcal{L})$ is defined as the change in enthalpy from liquid to solid is

$$\mathcal{L} = H_l - H_s \tag{3}$$

While Fourier's law of heat conduction,

$$\underline{q} = -k\nabla T, \tag{4}$$

So that we can substitute (4) and (3) into (2) and rewrite it as

$$\rho\mathcal{L}V_n = k_s \frac{\partial T}{\partial n}\bigg|_s - k_l \frac{\partial T}{\partial n}\bigg|_l \tag{5}$$

This is the Stefan condition (**?**). In this ideal case, the density of the solid and liquid are assumed to be the same. In the case of ice and water, $\rho_l > \rho_s$. A velocity is induced when

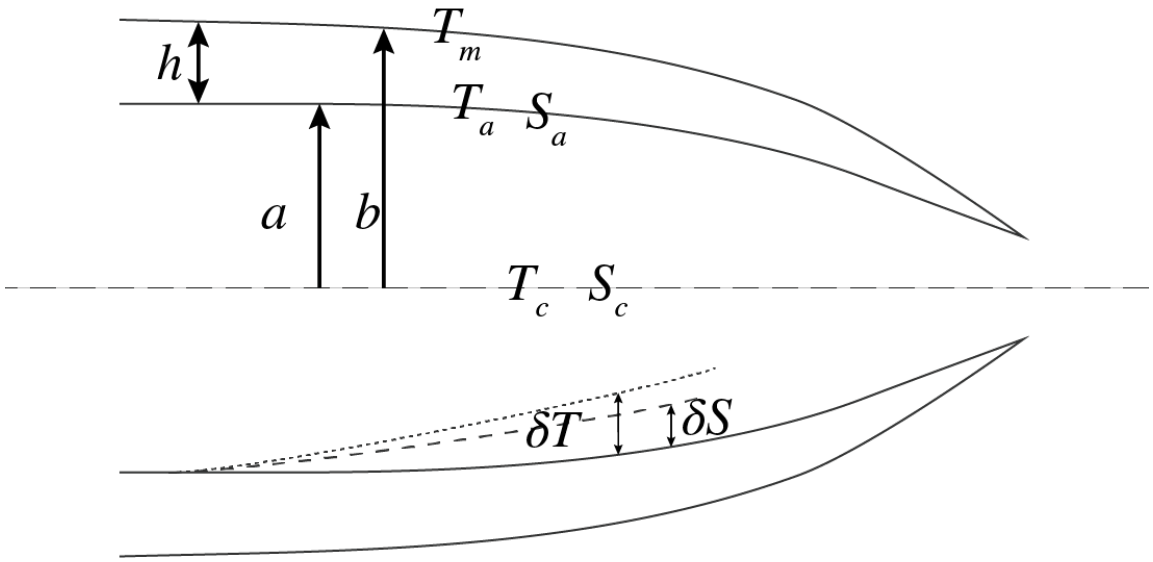

Figure 3.2: A schematic showing the boundary layers and variables used in the model.

the ice that freezes expands, and we end up with the same Stefan condition as above, but only dependent on ρ_s (**?**).

In the brinicle, there are two moving boundaries both at the inner wall and the outer wall. The inner wall moves as the warmer brine dissolves the wall, and the outer wall moves as heat is transferred to the brine on the inside and the fresh water freezes.

We write and simplify the radial heat equation inside the ice:

$$\frac{\partial T_i}{\partial t} = \frac{k_i}{r}\frac{\partial}{\partial r}\left(r\frac{\partial T}{\partial r}\right) + k_i\frac{\partial^2 T_i}{\partial z^2} \tag{6}$$

The temperature through the wall is quasi-steady, so $\frac{\partial T_i}{\partial t} = 0$. Since $\Delta x \gg \Delta r$, the dominant heat transfer is radial, so we also neglect z-dependence, and the heat equation simplifies to

$$\frac{\partial}{\partial r}\left(r\frac{\partial T_i}{\partial r}\right) = 0 \tag{7}$$

The boundary conditions at both the outer and inner walls are given by

$$\frac{\partial T_i}{\partial r} = \frac{\mathcal{L}\rho_i}{k_i}\frac{\partial b}{\partial t} \quad \text{at} \quad r = b(t), \tag{8}$$

At the outer wall, and

$$k_i\frac{\partial T_i}{\partial dr} = L\rho_i\frac{\partial a}{\partial t} + k\frac{\partial T}{\partial r} \quad \text{at} \quad r = a(t), \tag{9}$$

At the inner wall.

Solving equation 7 and substituting equations 8 and 9 into the heat flux at the inner wall

$$\frac{\mathcal{L}\rho_i}{2k_i}\frac{1}{a}\frac{\partial}{\partial t}(b^2 - a^2) = \frac{k}{k_i}\frac{\partial T}{\partial r}\bigg|_{r=a(t)} \tag{10}$$

This gives us an equation for the growth of the wall in terms of the heat flux. The heat flux appears on the right side of equation 10, and the time-derivatives of both a^2 and b^2 appear on the left side.

Having solved for the radial growth, we now focus on the moving tip. We must consider how heat is transferred with the flow of brine down the tube at the center of the brinicle. The Graetz problem solves for the temperature in a pipe with Poiseuille flow and constant heating of the walls (Martin, 1974). The solution gives us that mean temperature rises linearly with length down the pipe. In order to use this solution, we therefore assume that the heat flux into the brine is independent of height and that the temperature rises linearly from entrance to tip. We take this solution, and plug in our Poiseuille flow profile to get,

in non-dimensional co-ordinates, where θ is our non-dimensional temperature $\theta = \frac{T_m - T}{\Delta T}$

$$(1 - r^2)\frac{\partial \theta}{\partial z} = \frac{1}{r}\frac{\partial}{\partial r}\left(r\frac{\partial \theta}{\partial r}\right) \tag{11}$$

We apply boundary conditions at the side wall, entrance, and tip of the brinicle. At the entrance, the brine is at a constant temperature and volume flux, which gives us the condition

$$T_A = q(\Delta T)\alpha \quad \text{at} \quad z = 0, \tag{12a}$$

Where T_A is the averaged temperature, ΔT is the temperature difference across the wall of the brinicle, and α accounts for the fact that not all ice crystals that form become a part of the brinicle; some simply float to the top of the tank.

As discussed previously, the heat flux from the side at any height is only a function of time, which we represent as follows, using the same dimensionless variables

$$\frac{\partial \theta}{\partial r} = \frac{1}{4}B(t) \quad \text{at} \quad r = 1 \tag{12b}$$

As the tip is a moving boundary, we have to provide two boundary conditions. First, the temperature of the brine is the same as the temperature of the tank at the tip:

$$\theta = 0 \quad \text{at} \quad z = l, r = 1, \tag{12c}$$

Second, the tip grows as a cylinder of constant cross-sectional area. The cross-sectional area of the tip is $\pi(b^2 - a^2)$, and so we have the following equation for the growth of the

tip, up to a constant of proportionality

$$\pi(b^2 - a^2)\frac{\partial l}{\partial t} = \theta_A(l), \tag{12d}$$

After solving equation 11 for the given boundary conditions (12), Martin (1974) finds that the tip of the brinicle moves as a power law of t: $l(t) = \beta\sqrt{t}$, where β depends on the cross-sectional area of the tip, the ratio of the flux of ice to the flux of fluid into the brinicle, and the thermal diffusivity.

While the fluid that we pump into the tank is at a constant salinity and temperature, as the brinicle grows, the wall of the channel grows as the salty brine dissolves the ice. As this happens, there is a layer of fresher water along the outside of the channel. This layer is both at a different temperature and salinity than the water at the center of the channel. This boundary layer of fresher, warmer water grows as the brine flows through the channel, to the point where the stream exiting the brinicle is at the same temperature as the surrounding water. Throughout, we assume that this boundary layer is of a constant thickness.

We start with the Stefan condition

$$\rho\mathcal{L}\dot{a} = k\frac{\partial T}{\partial y} \tag{13}$$

Here ρ is the density, $\mathcal{L}$ is the latent heat of fusion, T is the temperature and k is the thermal diffusivity. We have two moving boundaries, and we write the stefan conditions at each boundary. At the outer boundary, we have

$$\rho\mathcal{L}\frac{\partial b}{\partial t} = k\frac{T_a - T_c}{\delta_T} \tag{14}$$

At the inner boundary, we have both freezing and dissolving at the boundary, and so our Stefan condition looks like this

$$\frac{T_m - T_a}{h} - \frac{T_a - T_c}{\delta_T} = \rho \mathcal{L} \frac{\partial a}{\partial t} \tag{15}$$

We write a similar condition for our moving inner boundary, but for the diffusion of salt, rather than heat:

$$S_a \frac{\partial a}{\partial t} = D \frac{S_c - S_a}{\delta_s} \tag{16}$$

We can combine (16) with (15) as follows, to get an equation that depends on both the diffusion of salt as well as heat

$$\frac{\rho \mathcal{L} D}{S_a} \left(\frac{S_c - S_a}{\delta_s} \right) = -k \frac{T_a - T_m}{h} + k \frac{T_c - T_a}{\delta_T} \tag{17}$$

Finally, using the liquidus on the binary phase diagram, we write the relationship between the T_m, the freezing temperature, and S the salinity. For this purpose we use a linear approximation **?**.

$$T_a = T_m - m S_a \tag{18}$$

We then have the following equations that describe our system.

$$\begin{aligned}
\rho\mathcal{L}\frac{\partial h}{\partial t} &= k\frac{T_a - T_c}{\delta_T}, && \text{(19a)}\\
S_a\frac{\partial a}{\partial t} &= D\frac{S_c - S_a}{\delta_s}, && \text{(19b)}\\
\frac{T_m - T_a}{h} - \frac{T_a - T_c}{\delta_T} &= \frac{\rho\mathcal{L}}{k}\frac{D}{\delta_s}\frac{S_c - S_a}{S_a}, && \text{(19c)}\\
T_a &= T_m - mS_a. && \text{(19d)}
\end{aligned}$$

Here (19a) corresponds to the diffusion of heat, (19b) to the diffusion of salt, (19c) to the diffusion of both heat and salt, and (19d) to the liquidus curve. We write the boundary conditions of the brinicle at the tip. We fix the width of the wall at 0 at the tip, and fix the inner radius as well.

$$h = 0 \quad \text{at} \quad x = \ell(t) \quad \text{and} \quad a = a_0 \quad \text{at} \quad x = \ell(t). \tag{20}$$

We now look for a traveling wave solution, with the brinicle moving at a constant velocity V, so that $\ell(t) = Vt$, i.e.

$$\xi = Vt - x, \tag{21}$$

where the tip is at $\xi = 0$ and the source is at $\xi = \ell(t)$. Plugging (21) into (19), our

equations transform to

$$\begin{aligned}
\rho\mathcal{L}V\frac{\partial h}{\partial \xi} &= k\frac{T_a - T_c}{\delta_T}, && \text{(22a)}\\
S_a V\frac{\partial a}{\partial \xi} &= D\frac{S_c - S_a}{\delta_s}, && \text{(22b)}\\
\frac{T_m - T_a}{h} - \frac{T_a - T_c}{\delta_T} &= \frac{\rho\mathcal{L}}{k}\frac{D}{\delta_s}\frac{S_c - S_a}{S_a}, && \text{(22c)}\\
T_a &= T_m - mS_a. && \text{(22d)}
\end{aligned}$$

We now nondimensionalize the equations as follows, leaving $\xi = L\xi$ such that we can determine L

$$T_a = T_m + \Delta T\theta_a, \quad \Delta T = T_m - T_c, \quad S_a = \Delta S C_a, \quad \Delta S = \frac{m}{\Delta T}, \quad a = \delta_T a, \quad h = \delta_T h,$$

we determine L as a grouping of parameters after nondimensionalizing the rest. Inserting these nondimensionalizations, this gives

$$\begin{aligned}
\frac{\mathcal{L}}{c_p\Delta T}\frac{V\delta_T^2}{L\kappa}\frac{\partial h}{\partial \xi} &= 1 + \theta_a, && \text{(23a)}\\
\frac{C_a V\delta_s\delta_T}{DL}\frac{\partial a}{\partial \xi} &= \frac{\Delta T S_c}{m} - C_a, && \text{(23b)}\\
\frac{\theta_a}{h} + 1 + \theta_a &= -\frac{\mathcal{L}}{c_p\Delta T}\frac{D}{\kappa}\frac{\delta_T}{\delta_s}\frac{\frac{\Delta T S_c}{m} - C_a}{C_a}, && \text{(23c)}\\
\theta_a &= -C_a. && \text{(23d)}
\end{aligned}$$

We define

$$\kappa = \frac{k}{\rho c_p}, \quad \epsilon = \frac{D}{\kappa}, \quad \mathcal{S} = \frac{\mathcal{L}}{c_p\Delta T}, \quad \mathcal{C} = \frac{mS_c}{\Delta T}, \quad Pe = \frac{V\delta_T}{D}, \quad b = \frac{\delta_s}{\delta_T}.$$

$\mathcal{S}$ is the Stefan number, defined as the ratio of sensible heat to latent heat; Pe is the Peclet

number, the ratio of the rate of advection to the rate of diffusion. Thus, we can choose that

$$L = \delta_T \mathcal{S}\epsilon Pe.$$

Now using the non-dimensional eutectic relationship in (23), we can write our equations only in terms of the non-dimensional 'concentration,' eliminating temperature as follows,

$$\frac{\partial h}{\partial \xi} = 1 - C_a, \tag{24a}$$

$$\frac{\partial a}{\partial \xi} = \frac{\mathcal{S}\epsilon}{b}\frac{\mathcal{C} - C_a}{C_a}, \tag{24b}$$

$$\frac{C_a}{h} - 1 + C_a = \frac{\mathcal{S}\epsilon}{b}\frac{\mathcal{C} - C_a}{C_a}. \tag{24c}$$

We write the large conglomeration of terms as

$$\mathcal{T} = \frac{\mathcal{S}\epsilon}{b} = \frac{\mathcal{L}}{c_p \Delta T}\frac{\delta_T D}{\delta_s \kappa}. \tag{25}$$

Writing the last equation of (24) as a quadratic of C_a, we have

$$(1+h)C_a^2 + (\mathcal{T}h - h)C_a = \mathcal{T}\mathcal{C}h. \tag{26}$$

Sending h to zero we find that the dominant balance must be between the first and last terms as

$$C_a^2 \sim \mathcal{T}\mathcal{C}h \rightarrow C_a \sim (\mathcal{T}\mathcal{C}h)^{1/2}. \tag{27}$$

Using the quadratic formula to solve for C_a we have that

$$C_a = \frac{(h - \mathcal{T}h) + \sqrt{(h - \mathcal{T}h)^2 + 4(1+h)\mathcal{T}\mathcal{C}h}}{2(1+h)}, \tag{28}$$

which agrees with the scaling as $h \to 0$.

The full system of equations is then

$$\frac{\partial h}{\partial \xi} = 1 - C_a, \tag{29a}$$

$$\frac{\partial a}{\partial \xi} = \mathcal{T}\frac{\mathcal{C} - C_a}{C_a}, \tag{29b}$$

$$C_a = \frac{(h - \mathcal{T}h) + \sqrt{(h - \mathcal{T}h)^2 + 4(1+h)\mathcal{T}\mathcal{C}h}}{2(1+h)}, \tag{29c}$$

subject to

$$h = 0 \quad \text{at} \quad \xi = 0 \quad \text{and} \quad a = \frac{a_0}{\delta_T} \quad \text{at} \quad \xi = 0.$$

Now we estimate the size of our terms for when we solve these equations.

$$\begin{aligned}
\kappa &\sim 1.4 \times 10^{-7}\ \text{m}^2\ \text{s}^{-1} \\
D &\sim 2 \times 10^{-9}\ \text{m}^2\ \text{s}^{-1} \\
\Delta T &\sim 20\ \text{K} \\
\mathcal{L} &\sim 3.34 \times 10^{5}\ \text{m}^2\ \text{s}^{-2} \\
c_p &\sim 4.19 \times 10^{3}\ \text{m}^2\ \text{s}^{-2}\ \text{K}^{-1} \\
\rho &\sim 10^{3}\ \text{kg}\ \text{m}^{-3} \\
m &\sim 0.5\ \text{K}\ (\text{wt.}\%)^{-1} \\
S_c &\sim 23\ \text{wt.}\% \\
\delta_s &\sim 2 \times 10^{-4}\ \text{m} \\
\delta_T &\sim 10^{-3}\ \text{m} \\
V &\sim 10^{-3}\ \text{m}\ \text{s}^{-1}
\end{aligned}$$

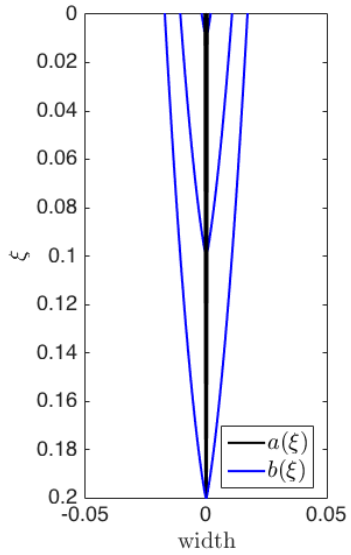

Figure 3.3: The outline of the brinicle, as solved for the model (29) at time steps 10, 100, and 200.

This gives that the parameters are

$$\epsilon \sim 10^{-2}, \quad \mathcal{S} \sim 5, \quad \mathcal{C} \sim 0.5, \quad Pe \sim 500, \quad b \sim \epsilon^{1/3} \sim 10^{-2/3} \sim 0.2, \quad \mathcal{T} \sim 5 \times 10^{-4/3} \sim 0.2.$$

We use MatLab to solve this system (29) of equations for $h(\xi)$ and $a(\xi)$. We can then plot the edges of the brinicle at various time steps as in fig. 3.3, and plot the width as a function of both time and height, as shown in fig. 3.4

4 Comparisons and Conclusions

The traveling wave solution of our model only solves for our brinicle with a tip that moves linearly in time. Therefore, we can compare the surface plot generated from the model to regimes of our experiment where we have close to linear growth. At the beginning of the

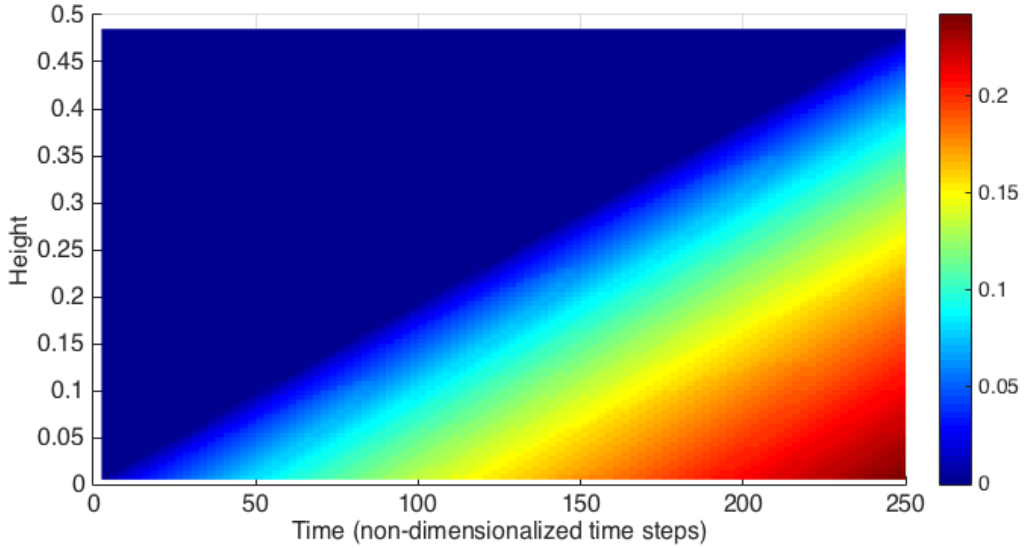

Figure 3.4: A surface plot showing the width of the modeled brinicle as a function of both the height and time. In non-dimensional coordinates.

growth of the brinicle in fig. 2.5a and fig. 2.5b. In the case of the brinicles grown in salt water (fig. 2.5b), we see even more similarities between the model and the actual data. We see large regions that look close to linear in time, for example, from 250-400 seconds. Particularly in this region, the width grows evenly without large deviations across the height, unlike in fig. 2.5a, where we see deviations in the width as a function of height, or as we referred to them earlier 'bumps'. Although to model the brinicle in salt water we have to add an extra term to the Stefan condition on the outer boundary (equation 14), when we compare our model to this data it does not make a huge difference. As we saw earlier from comparing brinicles grown in tanks of different salinities, adding salt does not affect the power law of the growth, and we see this is true for the width as well in comparing this model with the growth of brinicles grown in salt water. If we look at the plots of the brinicle grown in fresh water, we see that the bumps are what separates linear sections of this from the model. These bumps come from some deviation from the ideal

that then grows outward. When we add salt to the tank, these deviations no longer grow without bound the addition of the salt to the tank means that dissolution occurs at the outer boundary as well. Any small perturbations in the outer boundary would be dissolved by the salt before they could grow as in the fresh water tank.

In all these observations, as well as in the model, we see that the width continues to grow according the power law $\sqrt{t}$. However, according to Perovich et al. (1995), the brinicles they observed had a constant width throughout. The brinicles they observed were on a scale much larger than our scale – up to two meters. It appears that there may be another regime of growth in which the width does not grow or grows very slowly. Diffusion of heat is a slow process and as the brinicle grows in width it will eventually reach a width where the heat from the outer wall would diffuse too slowly into the brine on the inside to freeze and add onto the outer wall. Perovich et al. (1995) also observed that after a period of time the brinicles became less mushy, more solid, and were able to broken off, stored and observed properly. They also observed two different kinds of ice crystals: those that were radially oriented, and the more disordered crystals close to the center of the brinicles. In our experiments the brinicles grown in salt water never quite reached this phase. The brinicles remained fragile and broke when the block of ice fixed to the top of the tank was moved. We also only observed radially-oriented crystals. These are both clear in the photographs and videos, but also when the brinicles broke, there was no sign of a different kind of ice towards the center. Radially-oriented ice crystals were not present in the brincles grown in fresh water, and these were less fragile, so it is likely that the presence of more disordered ice adds more stability to the brinicle. While these are just empirical observations, one could follow Perovich et al. (1995) in quantifying the fraction of each type of ice inside the brinicle, and compare this with the stability or strength of the brinicle.

References

Paul K Dayton and Seelye Martin. Observations of ice stalactites in mcmurdo sound, antarctica. *Journal of Geophysical Research*, 76(6):1595–1599, 1971.

Seelye Martin. Ice stalactites: comparison of a laminar flow theory with experiment. *Journal of Fluid Mechanics*, 63(01):51–79, 1974.

National Snow and Ice Data Center. All about sea ice, 2017. URL `https://nsidc.org/cryosphere/seaice/index.html`.

Donald K Perovich, Jacqueline A Richter-Menge, and James H Morison. The formation and morphology of ice stalactites observed under deforming lead ice. *Journal of Glaciology*, 41(138):305–312, 1995.

Wilford F Weeks. Understanding the variations of the physical properties of sea ice. Technical report, DTIC Document, 1967.

M. G. Worster. *Solidification of Fluids*, chapter 8, pages 393–444. Cambridge University Press, 2000.